The Spacecraft Radiation Experiments

By W. L. BROWN, T. M. BUCK, L. V. MEDFORD, E. W. THOMAS, H. K. GUMMEL, G. L MILLER* and F. M. SMITS†

(Manuscript received March 22, 1963)

The radiation experiments on the Telstar spacecraft were designed to measure the electron and proton particle distributions in the region of space explored by the satellite orbit and to give information on the integral semiconductor radiation damage produced by these particles. A solar aspect experiment is included with the radiation experiments because of its direct importance to solar cell damage results. The design and the hardware for these experiments are described in the present paper. Results of the experiments are included in a companion paper in this issue.

I. INTRODUCTION

The radiation experiments on the Telstar spacecraft were designed to measure the distribution in energy, position, and time of electrons and protons trapped in the earth's magnetic field in the Van Allen belts. Such particle distributions characterize the radiation environment of the satellite, and in addition help provide an understanding of the mechanisms that are responsible for injection of particles into the Van Allen belts and for loss of particles from the belts. The radiation experiments also measure directly the integral radiation damage effects on semiconductors. Only magnetically trapped particles are important for damage considerations on the satellite, and only they are being examined in the particle experiments. The direct effects of primary cosmic rays are negligible, as are also the effects of solar protons which stream into the earth's polar regions but do not reach the Telstar satellite's extremes in latitude. However, these two classes of particles are important because of the secondary neutrons they produce in the earth's atmosphere, which subsequently decay in the trapped particle region and contribute both protons and electrons to the Van Allen belts.

Although the radiation belts have been examined in a large number of

* Brookhaven National Laboratory, Upton, Long Island, N.Y.
† Sandia Corporation, Sandia Base, Albuquerque, New Mexico.

experiments, the region of space traversed by the Telstar satellite has not previously been studied extensively. The satellite provides an unusually fine opportunity for quantitative observation of a large region that includes essentially the whole of the inner Van Allen belt as well as part of the high latitude "horns" of the outer belt. As it turned out, the satellite was to examine not only the natural particles in the radiation belts, as had been originally intended, but also particles artifically introduced into the belts by U. S. and Russian high-altitude nuclear explosions. These new particles were destined to play a major role in the radiation effects sustained by the satellite's electronic equipment.

The radiation experiments on the satellite are divided into those measuring radiation damage and those studying energetic particles. These will be discussed in detail in Sections III and IV, respectively. A solar aspect experiment which measures the orientation of the satellite with respect to the sun is also included as a part of the present paper, because it is essential to the radiation damage experiment on solar cells. It will be discussed in Section II.

II. SOLAR ASPECT

The attitude that the satellite presents to the sun is important for the performance of the solar cell power supply and for the temperature distribution of the satellite. The knowledge of this is also important for evaluation of the degradation of solar cells as a result of radiation damage, since changes in solar aspect affect the illumination of the cells whose output is being monitored. The satellite is spinning and, as a result, the satellite temperature and the average power from the solar power plant depend only on the angle α between the spin axis and the satellite-sun line, essentially the colatitude of the satellite-sun line with respect to the satellite. However, for a single solar cell or a group of cells which are parallel, the instantaneous output depends both on the colatitude of the satellite-sun line and its longitude φ with respect to the satellite. These two angles are determined in the solar aspect experiment.

The angles α and φ are determined by simultaneous measurement of the outputs of a group of six solar cells arranged as in Fig. 1. These cells have mutually perpendicular normals. In essence their directions are those of the faces of a cube. The three perpendicular axes defining the normals of the group could be located in any direction with respect to the spin axis of the satellite and still uniquely define the sun's position. For example, four cells could look out perpendicular to the spin axis and

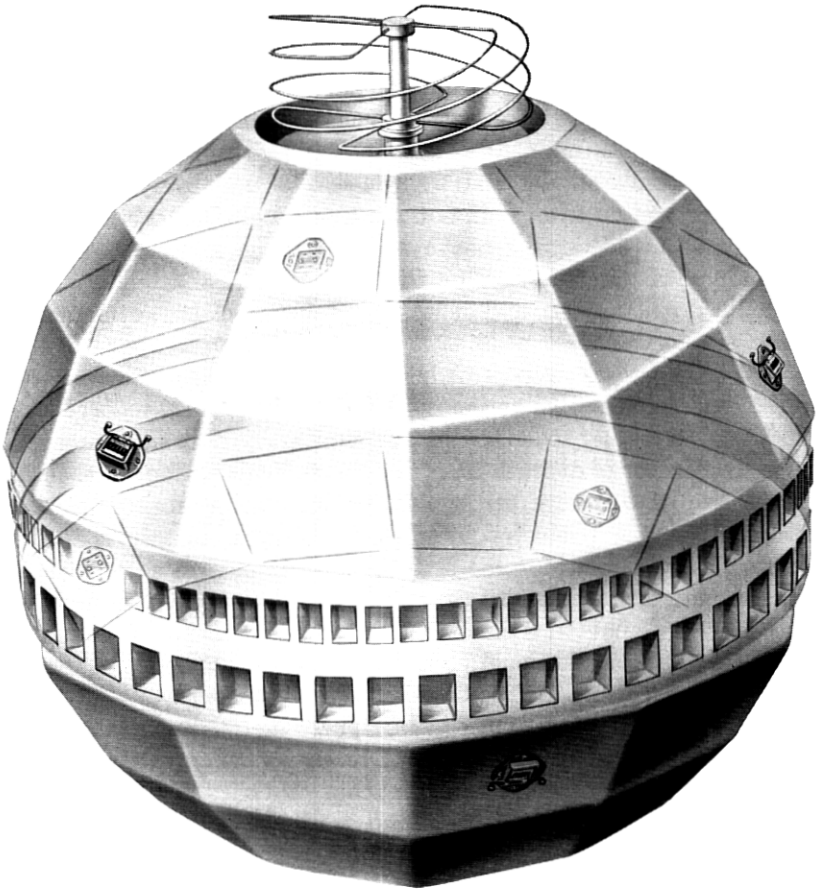

Fig. 1 — Placement of the solar aspect cells.

two in opposite directions along that axis. However, the arrangement of Fig. 1 has several advantages. The angle α is expected to be near 90 degrees, and reliable measurements near this angle are desired. With the cell positions of Fig. 1, one per cent measurements of the cell outputs define α and φ to one degree or better. Furthermore, as the instant of simultaneous measurement (determined by the telemetry frame rate) is not in general synchronous with the rotation rate of the satellite, the measurement of α depends in successive telemetry frames on different combinations of the six cells, so that failure or degradation of one is not disastrous.

The cells are mounted on the satellite facets nearest the antenna band to minimize the temperature extremes encountered as α departs from 90 degrees. The individual cells are of the same type (n-on-p) and are mounted with the same techniques used on the main solar power supply:[1] a ceramic base, platinum side strips and 30-mil sapphire covers. The cover width is much wider than a single cell, for uniformity in illumination and protection from radiation damage. Angle brackets orient the cell normals to 35 degrees above and below the satellite equator as required. With this mounting on the nearly spherical satellite surface, there are no shadowing and reflection problems of any consequence.

The six solar aspect cells were preirradiated with approximately 2×10^{16} 1-Mev electrons/cm^2 before mounting. This reduced their output under solar illumination by a factor of 2, but it reduced their sensitivity to further reduction in this number by radiation damage in space by a factor of at least 100.[1] The short-circuit current of each cell is measured as a voltage across a 2.75-ohm shunting resistor actually positioned in the telemetry interface circuitry inside the electronic canister. The currents for the six cells are sampled in a total of 600 microseconds, a time in which the satellite at its maximum rotation rate turns only by about one half of a degree. The timing is accurately known, so that an additional correction could be applied, but for this experiment the sampling is essentially instantaneous.

The telemetry examining the cell outputs has 100-millivolt full-scale sensitivity.[2] Changes in its gain are of relatively minor significance because the solar aspect angle really depends on ratios of the outputs of different cells. However, drifts in the amplifier zero would be quite serious. To provide a check on the zero, a seventh cell is placed inside the satellite skin and is covered with an opaque aluminum coating. To permit detection of zero drifts of either sign, a one-milliampere current is bled into the shunting resistor of this dark cell to offset its reading above zero by two telemetry bits.

The short-circuit current of an individual cell as a function of the angle of illumination with respect to its normal has been experimentally determined and is shown in Fig. 2. The shape does not depart substantially from a cosine law at small angles, but drops much more rapidly because of reflection losses toward grazing incidence. In addition to this calibration, interpretation of the telemetry readings to deduce the angle of illumination of a single cell involves temperature correction as illustrated by line A of Fig. 3. This is much larger than the temperature correction to the short-circuit current of nonirradiated cells, line B of the figure, because the recombination centers introduced by radia-

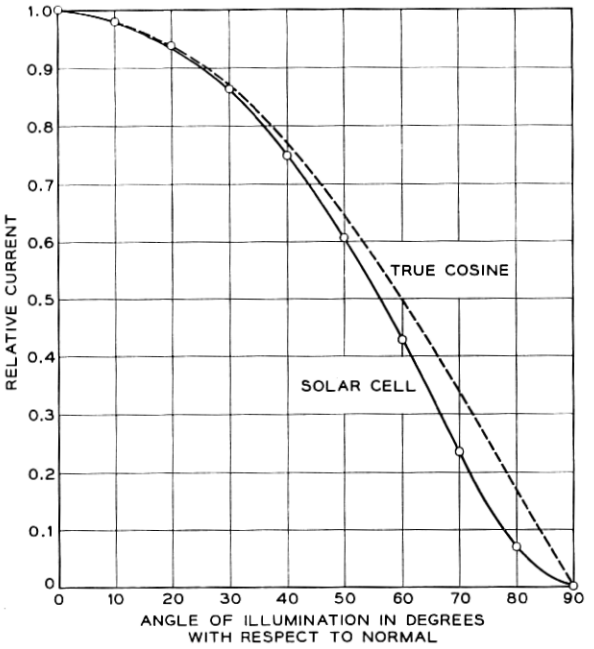

Fig. 2 — Solar cell short-circuit current vs angle of illumination.

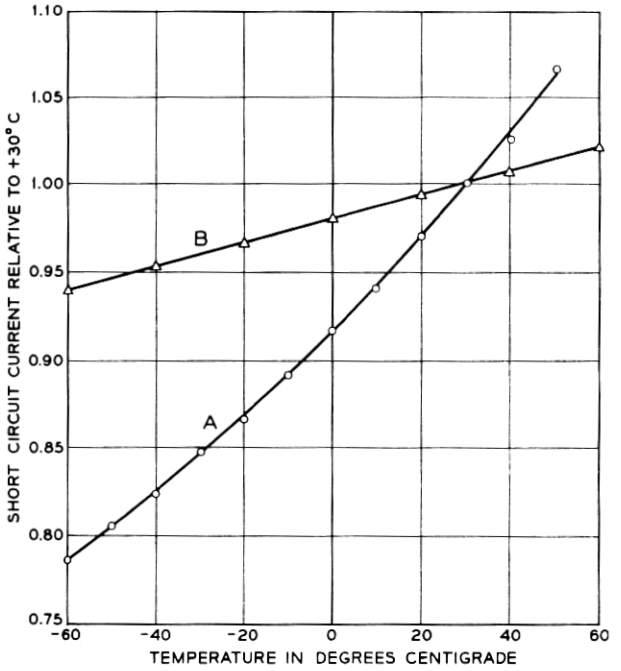

Fig. 3 — Temperature dependence of solar cell short-circuit current: (a) cell preirradiated with 2×10^{16} 1-Mev electrons/cm^2; (b) nonirradiated cell.

tion are quite different than those normally present. The operating temperatures in orbit range[3] from $-30°C$ to $+14°C$, but measurements have usually been made between $-10°C$ and $+5°C$.

Fig. 4 shows the anticipated output from the cells as a function of φ and for two values of α at 80 degrees and 90 degrees. In general, three cells are involved in the measurement, except at specific symmetry points where only two are illuminated, such as point A. The most critical measurement positions, those giving best definition to α and φ, are of type B, where three cells have substantial outputs and two are nearly alike. Such positions correspond to the sun being on the meridian of a cell in one hemisphere, and hence midway between the meridians of two cells on the other hemisphere. The ratio of the two nearly equal outputs to the one larger output is quite sensitive to α, and the ratio of the two nearly equal outputs to one another is very sensitive to φ. Because of the satellite rotation rate and its change with time, the sequence of one-minute measurements of the cell outputs will display a variety of patterns on different orbits of the satellite. Examples will be discussed

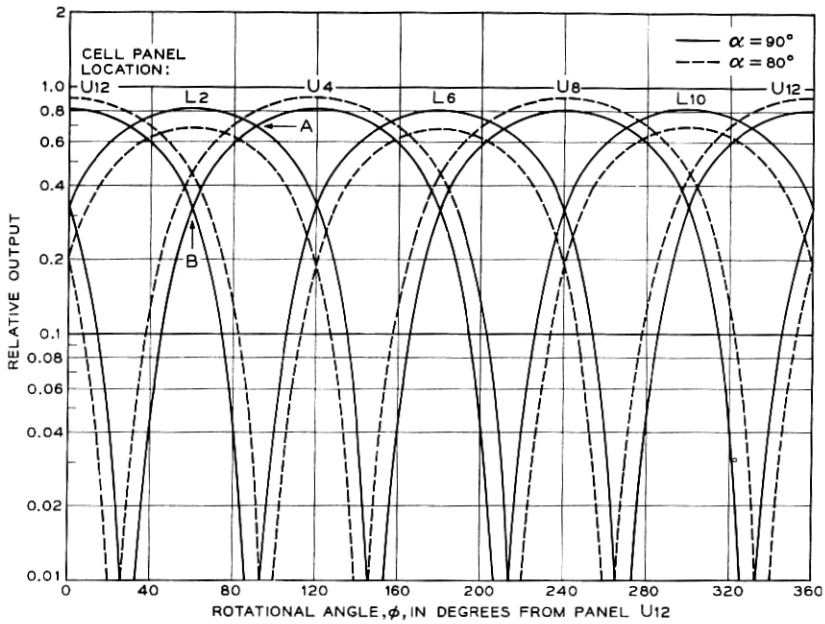

Fig. 4 — Anticipated dependence of the output of the solar aspect cells on the rotational angle of the sun with respect to the satellite for two different angles of the satellite spin axis with respect to the satellite-sun line.

in connection with the results of the radiation experiments in a separate paper.[4] The angle α can in general be determined from a single set of readings of the telemetry, but in practice many more points are used to avoid the possibility of error and to check on the reproducibility of the result obtained as different cells dominate in its determination.

III. RADIATION DAMAGE

3.1 *Solar Cells*

A solar cell damage experiment provides a direct measure of the degradation in short-circuit current due to radiation damage in three cells shielded by different thicknesses of sapphire. The cells are of the same type as the main solar power supply cells and the mounting is the same as for the solar aspect cells. It was not possible, using this mounting technique, to provide reliable attachment of thin covers, and hence the range in shielding thickness is narrower than would have been desirable. The cells are protected with 20, 25, and 30 mils of sapphire.

The group of three damage cells is mounted on the same facet of the satellite skin as one of the preirradiated solar aspect cells. This panel is shown in Fig. 5. The outputs of the damage cells are handled in the telemetry in the same way as those from the aspect cells, except that a 1.5-ohm resistor is used for a shunt because of the higher anticipated short-circuit current. The sampling time for the total of ten cells (six aspect, one zero-drift, three damage) is approximately 1100 microseconds.[2] The damage cells thus have the same illumination at the time of measurement as the solar aspect cell with the same orientation. With this arrangement, determination of changes in the unirradiated cells due to radiation damage can be made directly by comparison with that preirradiated aspect cell. The accuracy of the measurement depends markedly on the magnitude of all the outputs, but no correction for sun position is necessary in evaluating solar cell degradation. Furthermore, changes in illumination such as might arise from roughening of the sapphire surface by micrometeorites are not involved. Observation of the absolute current from the aspect cells measures this type of variation if it exists, although not distinct from changes in amplifier gain in the telemetry. Even if the aspect cell on the panel with the damage cell should fail, the redundancy of the determination of the solar aspect between remaining cells would make a continuing measure of damage possible without reliance on the absolute current. All of the cells in the aspect and damage parts of the experiment were measured with a spectral

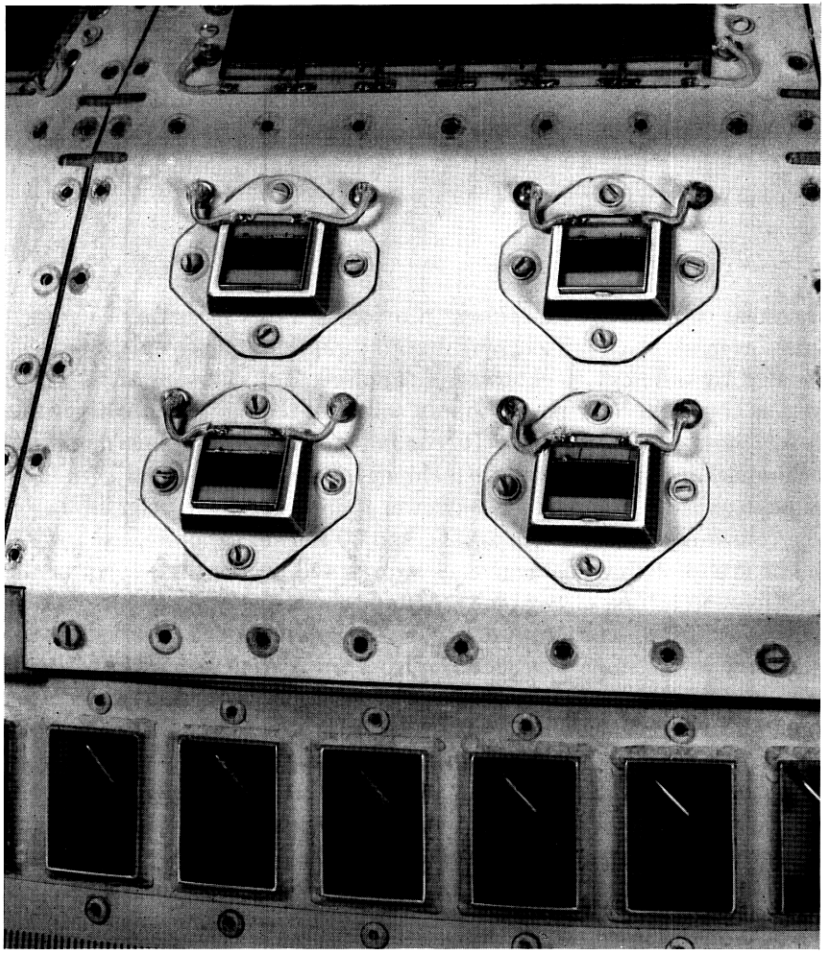

Fig. 5 — Radiation damage solar cell array. The lower right-hand cell is one of the six solar aspect cells.

analyzer developed by H. K. Gummel,[5] and predictions of their output under outer-space illumination were made. The shunt resistance choice was conservatively based on these measurements. For the damage cells the anticipated output was 52.5 milliamperes, the cells being similar within ±2 per cent. For the aspect cells, the predicted current was 23.5 milliamperes, with individual variations of less than ±3 per cent.

3.2 *Transistors*

To provide a direct measure of radiation damage in silicon independent of light, a group of npn diffused silicon transistors was specially fabricated. These devices provide a check on the solar cell results and permit extension of the study of shielding effectiveness to thinner shields. The degradation of solar cell performance under radiation results from a decrease in the lifetime of electrons (for n-on-p solar cells) in the p-type base material of the cell. This same property controls the α of transistors through the transport factor: the fraction of minority carriers introduced into the transistor base at the emitter which arrive at the collector junction. If lifetime is decreased by radiation damage, the light-created electrons (in the solar cell) and emitter-injected electrons (in the transistor) have increasing probability of recombination before they reach the solar cell junction or the transistor collector junction. Thus a direct comparison can be made between the results of one experiment and the other. As an experiment, the transistor has the advantage not only that the α measurement is independent of the sun, but also that the sensitivity to radiation damage can be made considerably greater by the use of a very wide base region.

The construction of the damage transistors is shown in Fig. 6. The device is made of the same kind of silicon used in solar cells (approximately one ohm-cm p-type) and the two junctions are made by solar cell junction diffusion techniques. These steps make a comparison of the results most direct. The transistor wafer is mounted on a pedestal close beneath the lid of the encapsulating Kovar can. For minimum shielding, the lid has been ground down to 3 mils from its normal 10-mil thickness. Through this thin lid the device sees particles over a 3.5-steradian solid angle.

The maximum sensitivity for damage measurement in transistors is limited by the maximum initial lifetime that can be maintained in the base region through device fabrication. The common-base current gain, α_{DC}, is related to the transport factor β across the base region as $\alpha_{DC} = \gamma\beta = I_c/I_e$, where γ is emitter efficiency, which we will assume to be independent of radiation damage. The lifetime τ of minority carriers in the base determines β in a device with base width W as

$$\beta = \operatorname{sech}(W/\sqrt{D\tau}) = \operatorname{sech}(W/L)$$

where D is a diffusion coefficient and L is the diffusion length for electrons in the p-type base. Radiation damage changes the lifetime[6] as

Fig. 6 — Construction of the radiation damage transistors.

$$1/\tau = 1/\tau_0 + K\Phi$$

where Φ is the integral flux of damaging particles and K depends on particle type and energy.

$$d\alpha/d\Phi = \gamma d\beta/d\Phi = -\frac{LK}{2D}\frac{W \sinh W/L}{\cosh^2 W/L}.$$

For small values of W/L, $d\alpha/d\Phi$ increases as W^2 for fixed L, the sensitivity to damage increasing with base width simply because the minority-carrier diffusion time increases and recombination processes become more evident. However, the expression has a maximum at $W \approx 1.5L$, corresponding to an α of about 0.43. Since τ_0 is limited by device processing, there is no advantage in increasing W beyond this point. In the damage transistors of the Telstar satellite, α is between 0.3 and 0.5 and the base width is on the order of 4 mils. As a result, the

devices have a low α cutoff frequency, about 100 kc. (Low-frequency cutoff and high damage sensitivity in transistors are almost invariably found together.[7] In examining components for potential susceptibility to damage, it is the low-frequency power devices that are of primary concern.)

The α_{DC} of the damage transistors is measured in the Telstar satellite in the circuit shown in Fig. 7. An approximately constant 0.5-milliampere dc emitter current is determined by the 8-volt zener diode and the 16.2-kilohm resistor in the emitter circuit. The extra diode in series with the zener partially compensates for change in the emitter current that would arise from the temperature dependence in the emitter junction. The collector current is read by the telemetry[2] as the voltage across the 16.2-kilohm collector resistor. With an α of 0.5, the output voltage has a maximum of approximately 4 volts. The output drops in proportion to α until it reaches the collector saturation current, specified in these devices to be less than 5 microamperes. This collector saturation current ultimately limits the minimum measurable α at two per cent of its initial value or less.

The relative change in α_{DC} in the transistors with radiation compared with the change in I_{SC} in solar cells is shown in Fig. 8. The initial rate of change of the transistor is somewhat greater, but even more striking is its continued high rate of change as the radiation proceeds. From the standpoint of a solar cell power supply, the decrease in the sensitivity to radiation with increasing damage is very helpful in providing extended life; but from an experimental standpoint, it makes evaluation of the damaging environment increasingly difficult.

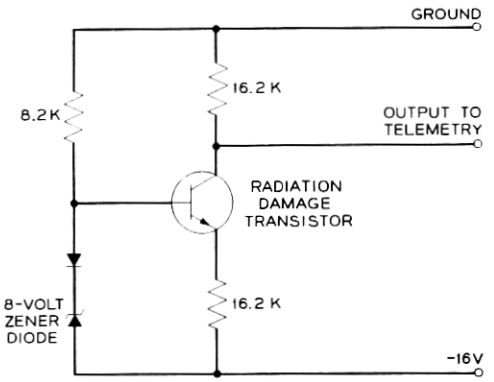

Fig. 7 — Radiation damage transistor circuit.

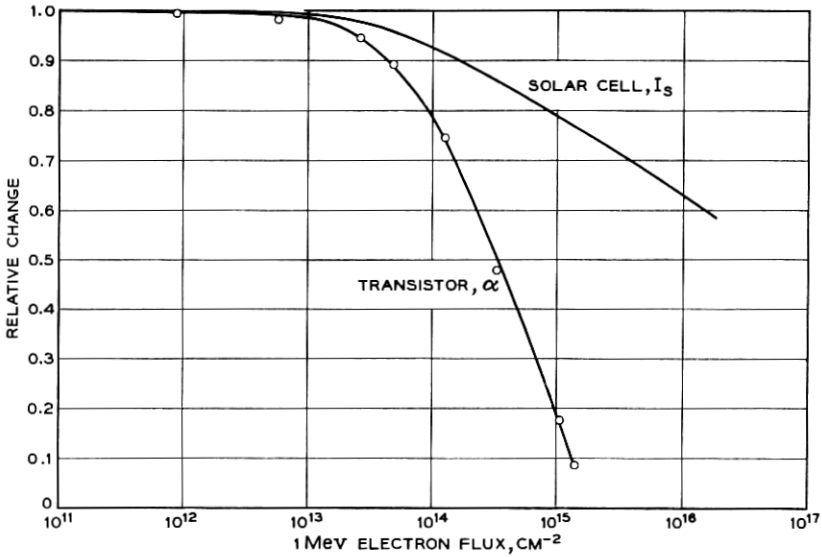

Fig. 8 — Comparison of radiation damage in solar cells and damage transistor.

Seven damage transistors are included in the transistor experiment, two each with three different shield thicknesses and a seventh which is heavily shielded and preirradiated to serve as a general check on the stability of the measurements. The devices and their associated circuits are assembled in a single package, shown in Fig. 9. This package (foamed and in a complete can) is mounted at a hole in the satellite skin, with its face almost flush with the surface of the satellite. The shield thickness of one of the pairs of devices, 35 mils of aluminum in addition to the 3-mil Kovar can, is comparable to the shielding of the main solar cell power supply, 30 mils of sapphire, and of one of the damage solar cells discussed in Section 3.1. The other two pairs have less shielding: 3-mil Kovar only and 3-mil Kovar plus 15 mils of aluminum.

IV. ENERGETIC PARTICLES

The Telstar satellite carries a group of four detectors designed to measure the spatial distribution and time variation of electrons and protons trapped in the earth's magnetic field and crude properties of their energy distribution. The satellite's orbit takes it through the most intense part of the inner Van Allen belt where protons of up to at least 500 Mev are known to exist[8] and where the proton flux increases with

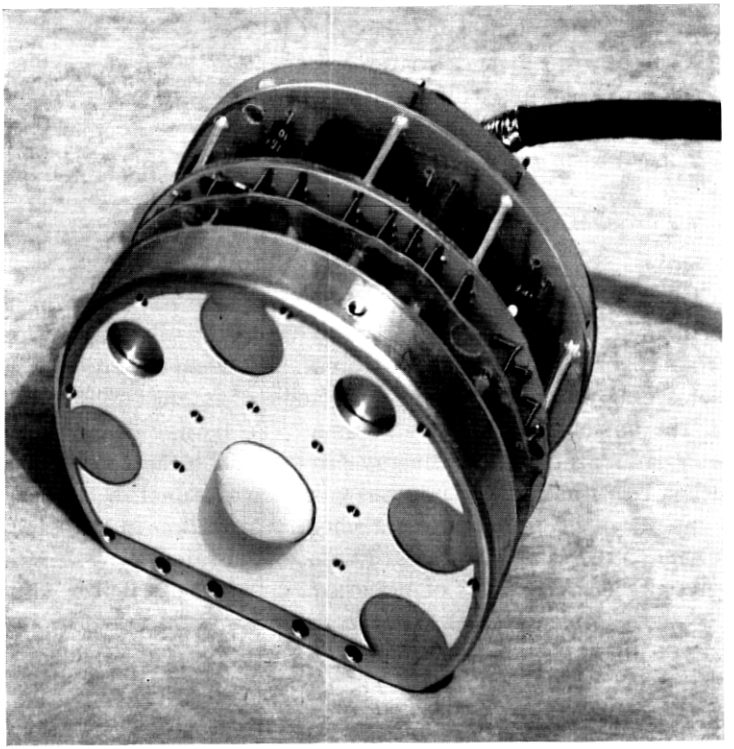

Fig. 9 — The radiation damage transistor assembly.

decreasing energy. The region also contains high fluxes of electrons whose intensity and energy distribution were poorly known. The orbit at high latitudes touches the horns of the outer Van Allen belt, which contains electrons and very low energy protons in concentrations that are highly variable as a result of solar activity.[9] One objective of the particle experiment is to establish a correspondence between the radiation damage in the solar cell power supply, the solar cells and transistors of the radiation experiment, and the distribution of particles responsible for the damage. Of even greater importance is the acquisition of data that will help provide a detailed understanding of the geophysical processes that produce and limit the radiation belts. Such an understanding is ultimately essential for assessing the radiation environment, not only in the Telstar satellite orbit but in other orbits of interest for communications satellite systems. In conceiving the experiments, no consideration was given to the possibility that effects of high-altitude

nuclear explosions might alter the belts in very significant ways,[10] although these artificial perturbations turned out to be of great importance. The next sections will describe the particle experiments, some details of the particle detectors, and some of the unique circuit features in the particle measuring experiments.

4.1 *The Particle Experiments*

The high particle intensity anticipated in the heart of the inner Van Allen belt requires the use of detectors which are fast and which have rather small geometrical factors (the product of the solid angle of particle acceptance and effective detector area). To avoid severe background problems that would arise if the solid angle of interest were made very small, the detector itself must be small. To permit discrimination of electrons from protons, some energy-proportional measurement is almost essential. To withstand the rigorous vibration of launch, a rugged device is required, and to provide for satisfactory operation in the vacuum of space, under the temperature variations of the satellite in orbit and in the presence of high levels of radiation, a device of great reliability is a necessity. Semiconductor particle detectors were selected as being nearly ideal. These are p-n junction devices which in effect are small solid-state ionization chambers.[11] They give output charge pulses proportional to the energy deposited by an incident charged particle in a disk-shaped active volume a few millimeters in diameter and a few tenths of a millimeter thick. They can be made with high reliability, as will be described in detail in Section 4.2. This kind of device has been extensively used in low-energy nuclear physics experiments in the last several years and provides high energy resolution[12] and relatively high speed.[13] In the Telstar experiment, the detectors are not being used as high-resolution devices or at their maximum capabilities of speed. Nevertheless, the nuclear physics experience with them has been invaluable in the satellite experiment design. Semiconductor detectors have been flown in the Injun and TRAAC satellites and in several Air Force satellites in the past two years, but very little of this information is yet available.

Three of the four detectors in the Telstar particle experiment measure protons, and the fourth measures electrons. Their energy ranges are:

low-energy protons	2.4–25 Mev
medium-energy protons	26–34 Mev
high-energy protons	>50 Mev
electrons	200 Kev–1 Mev (the detector response continuing to higher energies).

The outputs from the detectors time-share a single 14-bit register in the

telemetry, accumulating counts over periods between 3 and 15 seconds and reading out the register in all cases in two consecutive 7-bit telemetry words. The detectors are described individually in Sections 4.1.1 through 4.1.4.

4.1.1 *Low-Energy Protons (2.4 to 25 Mev)*

A cutaway view of the low-energy proton detector mount is shown in Fig. 10. The active p-n junction device is inside a transistor-like

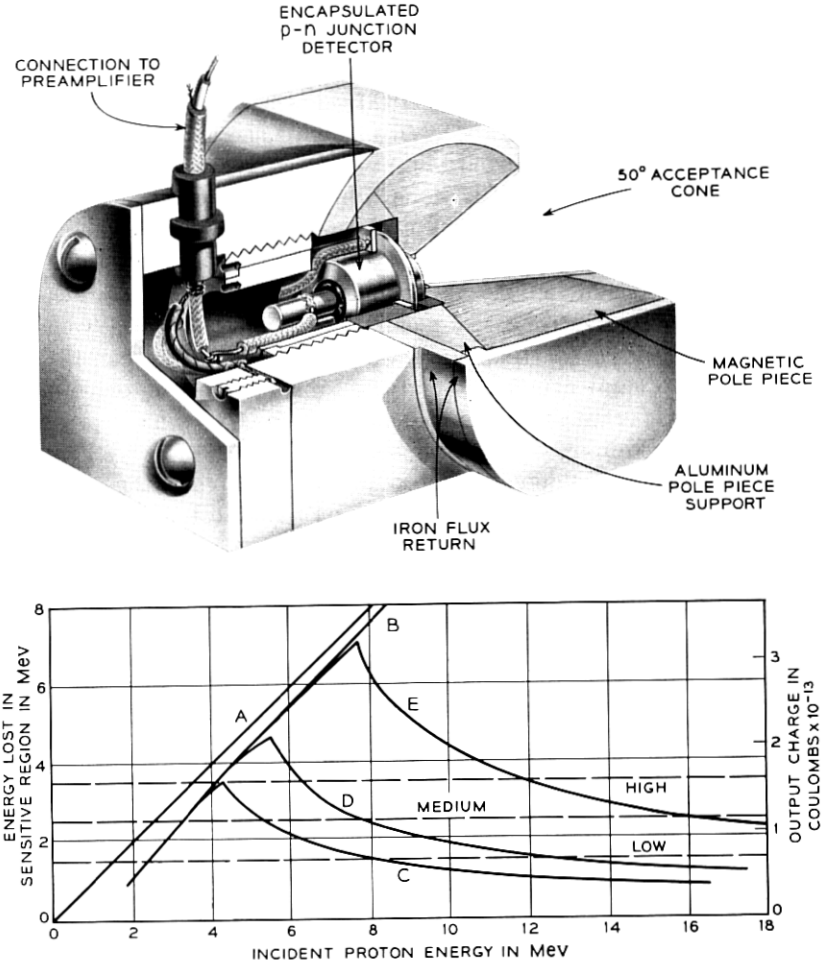

Fig. 10 — Cutaway view of the low-energy proton detector mount and the response of the detector to protons.

can (see Fig. 14, Section 4.2.1) surrounded by a relatively massive housing. The particles of interest enter through a cone with an acceptance angle of 50 degrees, truncated near its apex in an aperture 82 mils in diameter. Immediately behind this aperture is a Kovar window 80 mils in diameter and 0.3 mil thick which admits particles through the vacuum-tight enclosure of the detector encapsulation to the p-n junction device itself. Construction of this device is described in Section 4.2. The Kovar window excludes light, which would generate current in the device with high efficiency, and also removes protons with energies below 1.1 Mev and electrons below 15 Kev. A permanent magnet with tapered pole-pieces and a surrounding cylindrical soft steel magnetic flux return path provides a field in the acceptance cone that increases toward the apex and has a value of approximately 1500 gauss a quarter-inch from the detector. This magnet excludes electrons with energies below 300 Kev with increasing efficiency toward lower energies. It does so by deflecting them into the side walls of the cone, which is lined with aluminum to reduce electron back scattering. For electrons of 500 Kev or higher the magnetic exclusion efficiency becomes very low, and for all protons above a few Kev the magnetic field is insignificant in its effect. In directions outside the acceptance cone, the shielding of the detector is heavy enough to exclude protons of less than 80 Mev and electrons of less than 10 Mev. The detector mount extends behind the tubulation of the detector encapsulation to permit attachment of the detector to a coaxial preamplifier lead, still retaining the effective shielding.

The response of the detector to protons is illustrated in the lower half of Fig. 10. The electrical pulse developed by the detector is expressed in terms of the energy that an incident particle must leave in the detector to produce that pulse. One electron is available to the external detector circuit for each 3.5 ev of energy deposited by an energetic particle in the sensitive volume of the detector. This equivalence is independent of the particle type. The charge associated with an energy deposition is shown in the second vertical scale of the figure. The straight line A in the figure is a theoretical response just equal to the incident proton energy. The line B takes account of the effects of the 0.3-mil Kovar window and the diffused layer on the silicon detector, which together exclude protons of less than approximately 1.3 Mev and remove a smaller and smaller energy increment from protons of higher energy. The measured curves C, D and E correspond to three different effective detector thicknesses. This thickness is a little larger than the thickness of the p-n junction space-charge region — the region containing a high electric field. It is

variable with the bias on the detector. When the range of a proton just equals this thickness, the maximum energy loss and corresponding electrical pulse are obtained. For higher-energy protons less and less energy is left in the space-charge thickness. Curve C corresponds to a detector biased at 4.2 volts; D, 15 volts; E, 95 volts. The double-valued nature of each of these curves provides an energy band within which a pulse of a given size or larger can be observed. To change this band, either the sensitive thickness can be varied or the electrical pulse height discrimination level can be changed. In the low-energy proton detector, both of these variations are used. Nine distinct outputs can be obtained by measuring at each of three detector biases corresponding to curves C, D and E and by examining pulses within three different pulse height ranges marked by the horizontal lines on the figure: low, medium and high discrimination level.

The total span of energies covered by the detector is 2.4 to 25 Mev. However, it is not possible to measure a segment in energy close to the 25 Mev without including pulses from lower-energy particles as well. In a particle energy spectrum which falls rapidly with increasing energy, only an upper limit can be set on the number of the highest energy particles the detector is observing. The highest segment of energy which the present arrangement provides without a separate lower-energy component is that between 4.2 and 12 Mev, observed in the highest discrimination channel at the highest detector bias.

The probability that a single electron can produce a pulse as large as the 1.4 Mev of the lowest discrimination level is very small, less than one in 10^3. This is a result of the low rate of energy loss by electrons of this or higher energy. Pulse pile-up can occur from an anticipated high flux of low-energy electrons. The magnetic rejection reduces this problem for electrons of less than 300 Kev. Electrons of between 300 Kev and 600 Kev are of most serious concern. They are not well removed magnetically. They produce pulses comparable to their energy in many cases and pulse pile-up can reach the lowest discrimination level of the detector with only a three to fivefold multiplicity. A very high electron flux is needed to produce this pile-up, but a very high electron flux was measured in space during July, and the results of the low-energy proton detector consequently require careful examination.

The low-energy proton detector looks out perpendicular to the spin axis of the satellite through a hole in the satellite skin. It utilizes the single 14-bit register[2] in the telemetry for three seven-second periods during a one-minute telemetry frame, one period for the output of each

of the three discrimination levels. The detector bias is changed each frame, so that a complete sequence of nine readings requires three minutes.

4.1.2 *Medium-Energy Protons (26–34 Mev)*

The medium-energy proton detector mount is illustrated in Fig. 11. In this case the p-n junction detector is being used essentially on edge, particles of interest entering within a few degrees of perpendicular to the axis of the cylindrical detector disk and not nearly parallel to it as in the low-energy proton case. The acceptance aperture is a pair of 20-degree wedges like orange slices that have a common apex line through the junction device perpendicular to its cylindrical axis. This common apex line is parallel to the spin axis of the satellite. As the satellite makes half a rotation these wedges together sweep out a 4π solid angle. The detector is thus omnidirectional, sensing equally particles in all directions if its output is averaged over a time long compared to half a rotation of the satellite. As it is used, output pulses from the detector are summed for a 15-second period, corresponding to 45 complete rotations at the initial satellite spin rate. The detector protrudes through the skin of the satellite to permit essentially unobstructed access of particles to the wedges.

Protons penetrate this detector more or less along its diameter, and consequently can leave much larger amounts of energy in the space-charge region than was the case in the low-energy proton detector. The maximum path length is approximately 2.5 mm instead of about 0.4 mm as in the previous case. This makes it possible to set a high pulse height discrimination level, 11.4 Mev. No proton entering along the axis of the detector, or even at angles of up to 60° from the axis, can deposit enough energy to trigger this level. No electron is capable of triggering this level with any significant probability, no matter what its incident direction. Moderate shielding along the axis in the forward and back directions is used to remove problems of pulse pile-up, and very heavy shielding is used between 60° to the axis and the acceptance wedges to reject any protons of lower than 100 Mev. The detector should be extremely free from response to unwanted particles.

If the junction device were not surrounded by any material in the acceptance wedges, it would detect protons starting at an energy of 11.4 Mev. However, the thickness of the Kovar detector can wall (5 mils from the side) and an additional absorber placed within the acceptance wedges pushes this minimum energy up to approximately 26 Mev. The calculated detector response is shown in the lower part of Fig. 11. The curve represents the average response for protons incident over the ac-

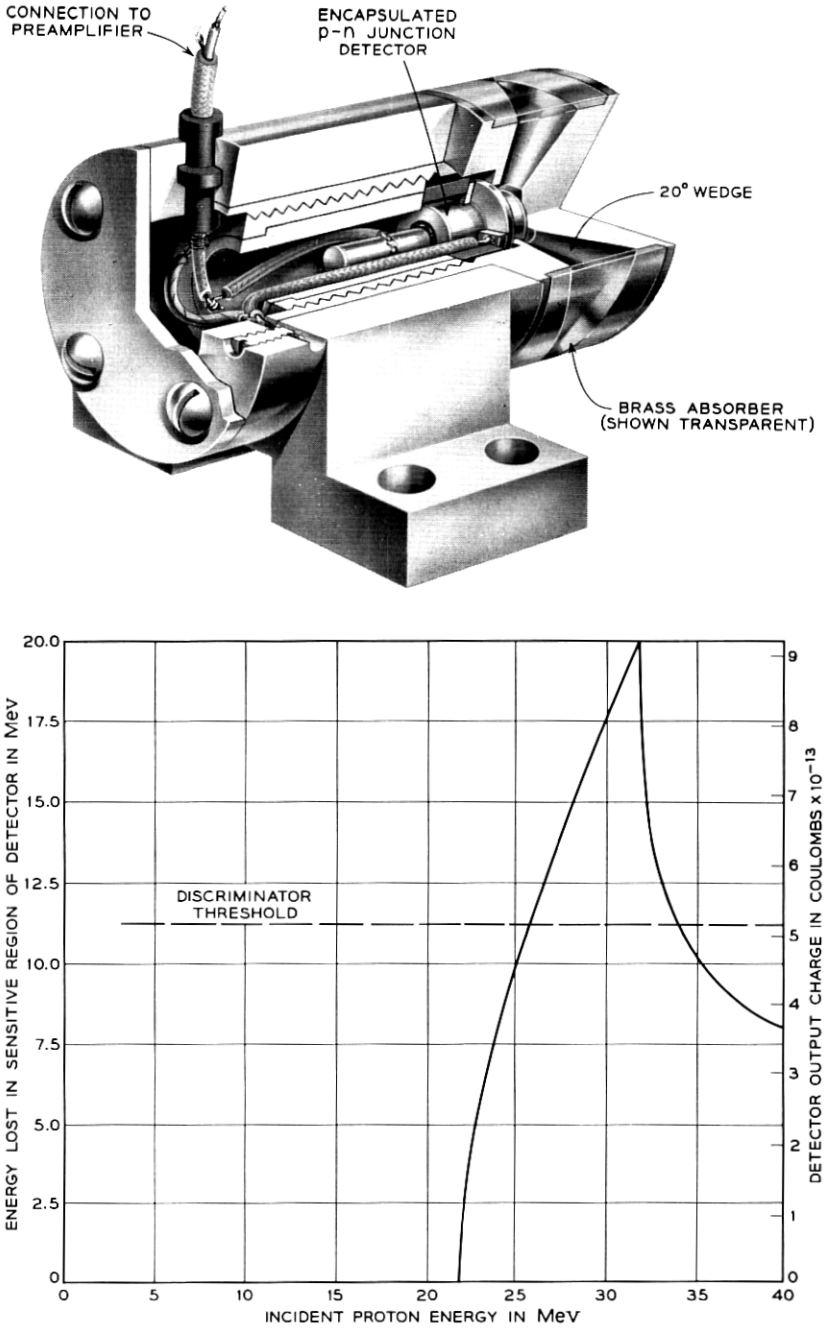

Fig. 11 — Cutaway view of the medium-energy proton detector mount and the calculated response of the detector to protons.

ceptance aperture. The shape for a particular angle of incidence and position of the particle path with respect to the disk diameter will vary because of the different path lengths the particles take. This detector supplies pulses from its single discrimination channel to the 14-bit register of the telemetry for a period of 15 seconds each telemetry frame.

4.1.3 *High-Energy Protons (>50 Mev)*

Energy discrimination in this detector is obtained by use of an absorber. The detector mount is shown in Fig. 12. The junction device is placed in the center of a hemispherical aluminum shell to provide an approximately uniform absorber over a 2π solid angle. The detector mount is inside the satellite skin, and taking into account the satellite structure near the detector, the effective threshold energy of the device is calculated to be approximately 50 Mev. The detector is not truly omnidirectional because of nonuniformity in the absorber thickness in different directions. However, because of the rotation of the satellite this lack of directional uniformity is largely averaged out. All pulses in the detector greater than 2.1 Mev are accepted. The calculated detector response for particles entering in a representative direction is shown in the lower part of Fig. 12.

The single discrimination channel of the high-energy detector makes use of the 14-bit telemetry register for 11 seconds of the one-minute telemetry frame.

4.1.4 *Electrons*

The electron detector mount is illustrated in Fig. 13. This mount protrudes through the satellite skin and looks out perpendicular to the spin axis. Particles are accepted in a cone having an angle of 20 degrees with an 82-mil diameter aperture immediately in front of the junction detector can. The deposition of energy by electrons in the sensitive volume of the detector is much less clearly related to the actual particle energy than is the case for protons. A 600-Kev electron may leave all its energy in a sensitive volume 0.43 mm thick (the thickness of the electron detector on the Telstar satellite); it may back scatter in the first fraction of this thickness and leave only a small part of its total energy; or it may penetrate entirely and leave less than all its energy to be detected. By examining the distribution of pulse heights produced in the detector, only a rough evaluation of the spectrum of incident electrons can be obtained, since the spectrum must be unfolded from the distribution of pulse heights produced by monoenergetic particle groups. (See Fig. 15, Section 4.2.3.1.) The probability that an electron of more

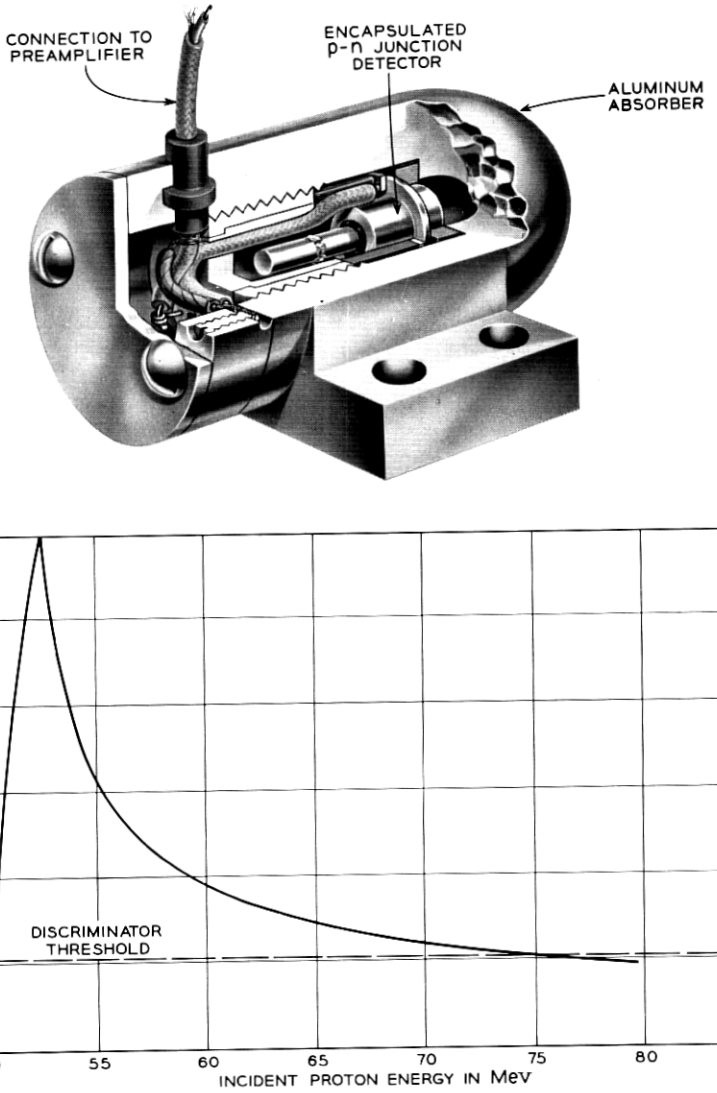

Fig. 12 — Cutaway view of the high-energy proton detector mount and the calculated response of the detector to protons.

than 1 Mev will leave all its energy in the sensitive detector thickness is very small. Such electrons can be detected by the lower energy pulses they produce, but their energy cannot be directly deduced.

In the Telstar electron detector, particle pulses are sorted into four pulse height channels: 180–280, 285–440, 390–615 and 635–990 Kev.

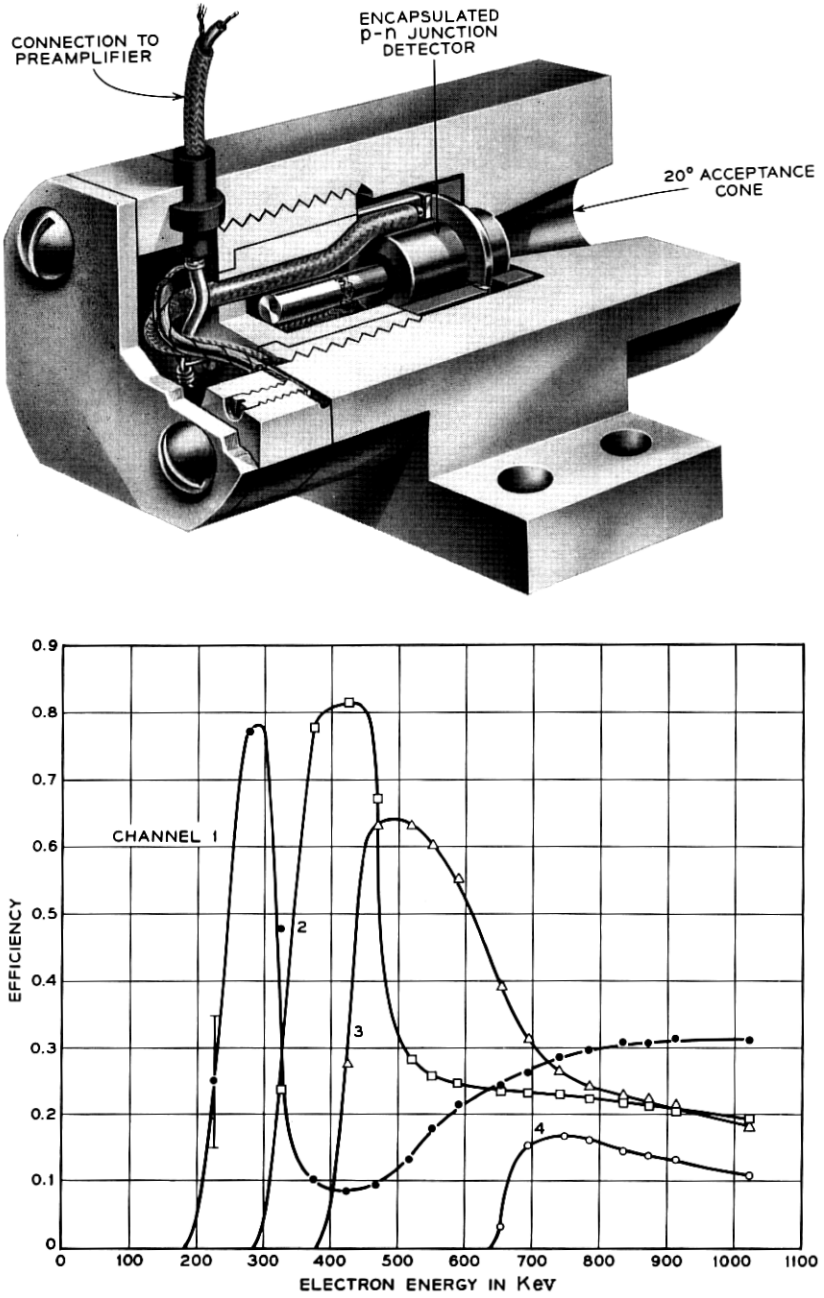

Fig. 13 — Cutaway view of the electron detector mount and the response of the detector to electrons.

The bottom edges of these channels correspond to 215, 315, 420 and 660 Kev, taking into account the energy lost by electrons in penetrating the 0.3-mil detector can window and an additional 1.6-mil aluminum absorber used to remove protons of less than 2.3 Mev. Pulses from two of the four channels are fed to the 14-bit telemetry register for three seconds each in every other telemetry frame. The second pair of channels, produced by a change in amplifier gain, is measured in the alternate frames.

The efficiency of each of the four channels for counting electrons up to approximately 1 Mev is illustrated in the lower part of Fig. 13. Each channel starts abruptly as the energy requirement of the channel is met, but retains a substantial efficiency at electron energies above the upper pulse height limit of the channel.

The electron detector is potentially susceptible to background problems from protons. The addition of the 1.6-mil aluminum absorber eliminates the problem for very low energy protons. In addition, the top pulse height channel is closed. Pulses in excess of 990 Kev will not be counted. To be recorded, protons must have energies greater than 2.4 Mev to penetrate the entrance window and leave at least 180 Kev in the detector, but energy less than 2.7 Mev, so they do not leave more than 990 Kev (a shield that just stops 2.3-Mev protons will extract less than 2.3 Mev from 2.7-Mev protons). This very narrow energy range for proton acceptance makes the proton contribution to the counting rate small except when the electron flux nears the minimum values that it has in the Telstar satellite's portion of space.

4.2 *Silicon p-n Junction Detectors*

Silicon p-n junction detectors were used in all the particle experiments, as described in Section 4.1. They satisfy the requirements of small size and rugged construction, high sensitivity, high speed, low noise, and in addition provide high reliability in the space environment where temperature and radiation intensity vary continuously. The construction and testing of these detectors will be discussed in the following sections.

4.2.1 *Mechanical Construction*

Surface reliability was recognized as a problem of major proportions in designing the Telstar satellite detectors. Surface control was achieved by adopting a hermetically sealed transistor-type encapsulation with a thin window. Such a window was permissible in this experiment, although it would not be for many nuclear physics experiments. The design which evolved is shown in a schematic cross-sectional view in Fig. 14. The

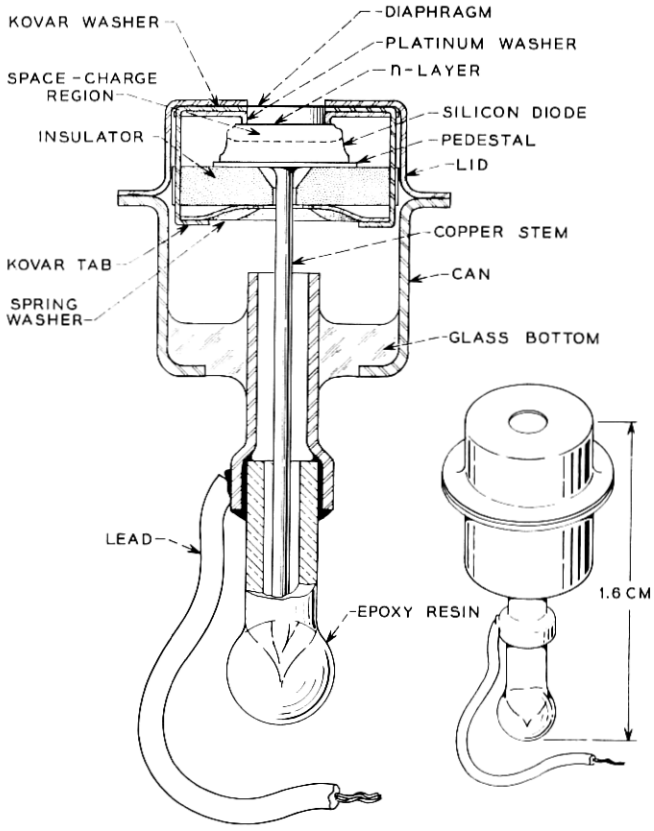

Fig. 14 — Cross-section view of encapsulated detector.

encapsulation consists of a Kovar can with a glass bottom and a metal tubulation, and a Kovar lid which is welded onto the can in final assembly. All Kovar parts are gold plated. The diode with the diffused n-layer looks out through the hole in the lid, which is covered by a Kovar diaphragm which may be as thin as 0.3 mil. The diaphragm is welded between the lid and a Kovar washer to make a good vacuum seal. The diode is pressed against a platinum washer which has a raised rim around the hole and thus provides contact to the n-layer. Contact to the back or p-region of the diode is made through the gold-plated Kovar pedestal alloyed to it. A good low-resistance contact is needed here to provide a pulse rise time of less than 0.2 μsec. A copper stem completes the connection to the tubulation and a stranded lead makes contact to it.

The p-region of the diode is insulated from the main body of the encapsulation by a ceramic insulator. A spring washer is compressed against the insulator by tabs which extend from the Kovar washer welded to the lid. After assembly the device is evacuated, baked at 200°C for an hour or more, cooled to room temperature, back filled with a suitable atmosphere and the tubulation pinched off. A drop of epoxy resin is used to protect the delicate feather edge of the pinch off.

4.2.2 *Materials and Processing*

The detector diodes are of the n-on-p type,[14] made by diffusing phosphorus into silicon of the highest available resistivity, i.e., about 10,000 ohm-cm to 20,000 ohm-cm. At 100 v the space-charge depth in this material is 0.30–0.45 mm. Deeper sensitive regions could have been obtained by using the lithium-drift technique[15] which produces a p-i-n structure with very close compensation in the middle, drifted region. However, preliminary tests showed that Li-drifted diodes are much more rapidly degraded by radiation damage than are the n-on-p diffused diodes and would have too short a life in the radiation environment the Telstar satellite was expected to encounter. They also exhibit a more complicated surface behavior.[16] The phosphorus diffusion is carried out at 1050°C, using P_2O_5 in an open tube system. A diffusion time of three hours gives a junction depth of about 4 microns. This "dead layer" or "window" is negligible compared to the thickness of the Kovar diaphragm. After diffusion, the slices are wafered and the small diodes then alloyed to pedestals, etched and encapsulated.

4.2.3 *Performance and Testing*

4.2.3.1 *Calibration and Counting Behavior.* Direct calibration of the particle detectors was carried out with electrons from a 1-Mev Van de Graaff generator and also with 17-Mev protons from the Princeton cyclotron.* Fig. 15 shows pulse height spectra for electrons of 5 different energies, taken on a detector with 100-v bias. These results differ only slightly from those corresponding to the 95-v detector bias in the satellite. It may be seen that the total absorption peak is quite high for 220 and 425-Kev electrons and then becomes progressively smaller until it has almost disappeared at 990 Kev. At the same time, a broader peak due to electrons which lose only part of their energy in the space-charge

* These calibrations were carried out with the kind cooperation of Professor R. Scheer of the Princeton University Physics Department.

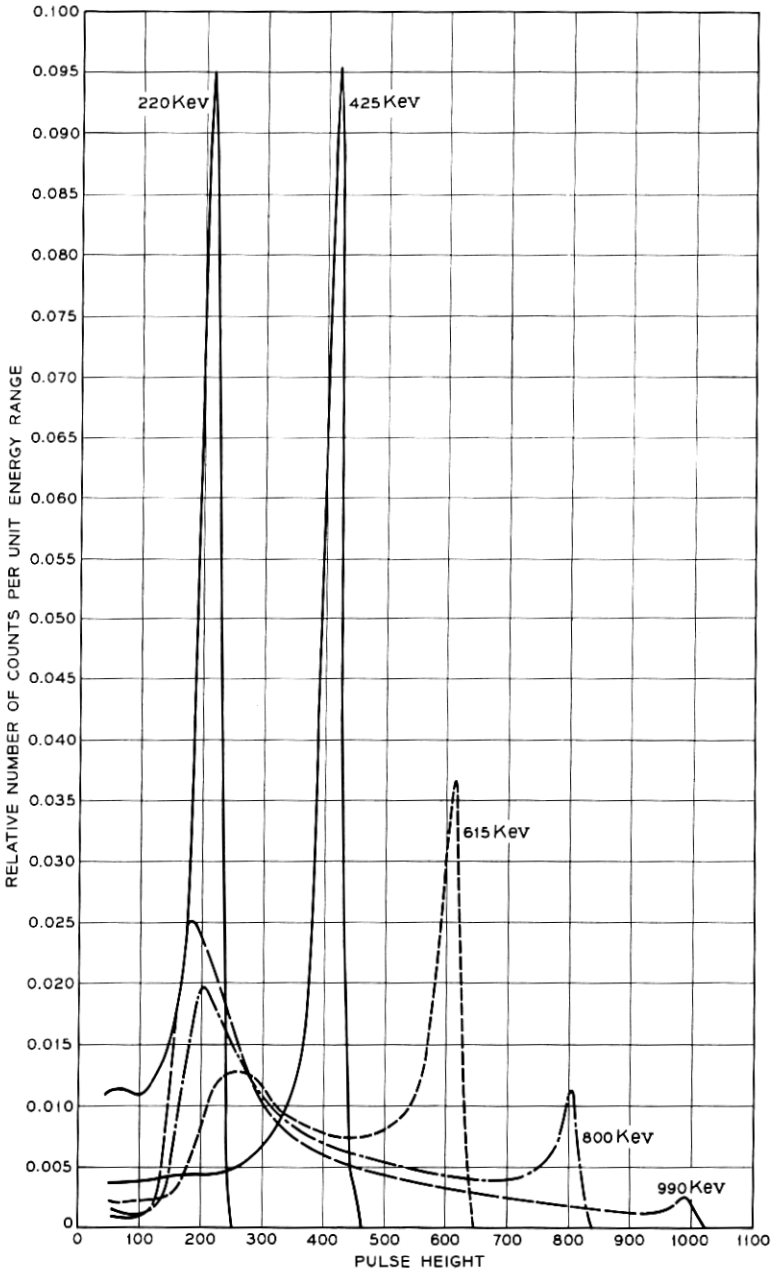

Fig. 15 — Pulse height spectra for electrons of five different incident energies. Pulse heights are indicated in terms of energy deposited by an electron in the sensitive region of the detector.

region is increasing in size.* By calibration with protons which, unlike electrons, have a precisely defined range at a given energy, the depth of this detector was found to be approximately 0.43 mm at 100 v.

Detector noise is an extremely important characteristic of the junction detector, particularly in the case of the electron detector, where pulses corresponding to particle energy losses in the detector of less than 200 Kev are to be measured. Spurious noise pulses which even approach this threshold level are serious because of the distortion they produce in the pulse height distribution. The noise in low-noise devices can be examined most easily, not in terms of the probability of finding a spurious pulse equivalent to 200 Kev, but as a broadening in the distribution of pulse heights produced in response to a series of uniform electrical pulses artificially introduced in the detector. The full width at half height of this pulse height distribution is measured and expressed in terms of an equivalent particle energy. Such noise linewidth measurements were obtained in all detectors under standard conditions, and in a number of cases whole sequences of noise measurements were made through a series of environmental tests.

4.2.3.2 *Reliability*

i. Surface Reliability. The essence of the surface reliability problem on the detectors is illustrated in Fig. 16, in which reverse current is plotted against bias for three representative cases. These curves were measured on different encapsulated units which were all good initially but which aged in different ways to arrive at the conditions shown. Curve A is a typical good, low-noise characteristic which is obtained with the surface (of the high resistivity p-side) nearly intrinsic or perhaps slightly n-type.[18] The current is 0.14 μa at 100 v and noise linewidth was 10 Kev. (Note that the current scale for A differs by a factor of 100 from that for B and C.) Curve B results from a strong n-type inversion layer over the p-region. The current is 48 μa at 100 v and the noise linewidth 85 Kev. The behavior depicted by curve C is due to an accumulation layer at the surface; i.e., the surface is more strongly p-type than the bulk. The charge in surface states is negative, and the resulting high field at the edge of the junction causes surface breakdown at many little spots around the junction. Even at 1 v, where the current is only 0.04 μa, the noise linewidth is 90 Kev, and at 5 v bias the noise is greater than 450 Kev. The diode represented by this type of characteristic is the noisiest of all for a given current. There is very good correlation between

* These results are similar to those of Ref. 17.

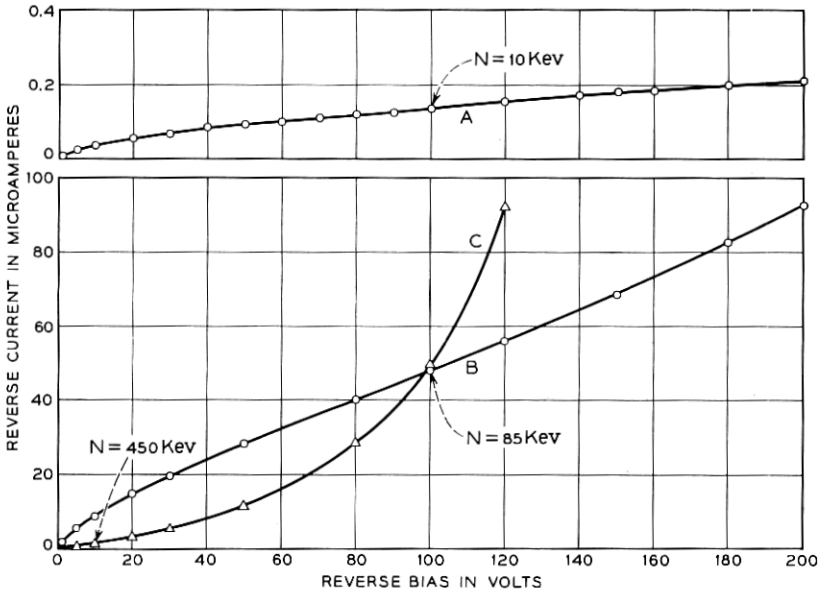

Fig. 16 — Typical reverse current-voltage characteristics for detector diodes with: (a) normal low-noise characteristic; (b) strong n-type inversion layer; (c) p-type surface accumulation layer. Note smaller scale for A. Noise linewidth values N are indicated at particular points on the curves.

noise and I–V characteristics* that has made it possible to predict noise by inspection of an I–V curve. Even a small departure from curve A toward the B or C conditions shows up as an increase in noise.

The maximum permissible noise linewidth was about 50 Kev for the electron detector, and several hundred Kev for the proton detectors. Newly fabricated detectors were all well below this, at about 10–15 Kev, but many of the early models developed poor I–V characteristics and high noise within a few weeks on shelf aging. Of the first 100 produced, only 44 survived after a few weeks. Transistions between characteristics of the type illustrated in Fig. 16 may be brought about very quickly by atmosphere changes or wet chemical treatments which shift the surface potential in known ways,[19] but the causes of long-term shifts on shelf aging, bias aging and temperature cycling are harder to detect and control. Nevertheless, by careful adjustment of surface potential by initial chemical treatments and by control of the ambient atmosphere

* Early studies of noise in the detectors were made in collaboration with H. C. Montgomery and L. K. Monteith. See also Ref. 16.

in the encapsulations it was possible to improve the yields to about 90–95 per cent by the end of the project. The processing will be described more fully in another paper.[20]

Indirect effects of radiation on the detector surfaces as a result of ionization of the ambient gas within the encapsulating can were considered, since such effects had recently been observed on transistors.[21] Selected groups of detectors were tested under intermittent bias and continuous bias in γ radiation of 50 rads/hr, approximately the average encountered in space. In general the effects have been rather small, although complicated. Changes do occur when the conditions are changed; as the bias or radiation is turned on or off the currents may increase or decrease, but after a few days in a new condition the current levels off at a new steady-state value. Detectors vary in their sensitivity to radiation for reasons not yet understood, but not many are severely affected by radiation at this dose rate level.

ii. Bulk Radiation Damage Effects. The effects of particle radiation on bulk properties of the detectors are not yet well understood, although it can be said that really serious effects are not expected in less than about a year. After a bombardment with about 10^{14} electrons/cm^2 of 1-Mev energy, a loss in pulse height begins to appear. The electron detector in the Telstar satellite has received damaging particles equivalent to about 5×10^{11} 1-Mev electrons/cm^2 day. On this basis one may expect that the electron data will begin to be affected by bulk damage after about six months in orbit, and that thereafter it may be necessary to estimate corrections by using damage measurements obtained on the ground. The low-energy proton detector, with the largest solid angle and the thinnest diaphragm, may be affected somewhat sooner. The medium and high-energy proton detectors with their thick shielding will not be affected until much later.

iii. Life Testing Program. Finished detectors were put through a life testing program which included:

(a) Vibration at frequencies from 50 to 2000 cycles/sec and accelerations of either 40 or 80 g's in both the longitudinal and transverse directions. Two typical detectors were subjected to 12 shock tests with successively higher accelerations, up to 1100 g, without any apparent damage.

(b) High humidity soaks at 95 per cent RH for 16 to 24 hrs, followed by vacuum pumping and exposure to oxygen. The surface sensitivity of the diodes is such that any leak would be easily detected by this test.

(c) Temperature and bias cycling in a vacuum chamber for at least one month. Temperature was cycled continuously from -50°C to

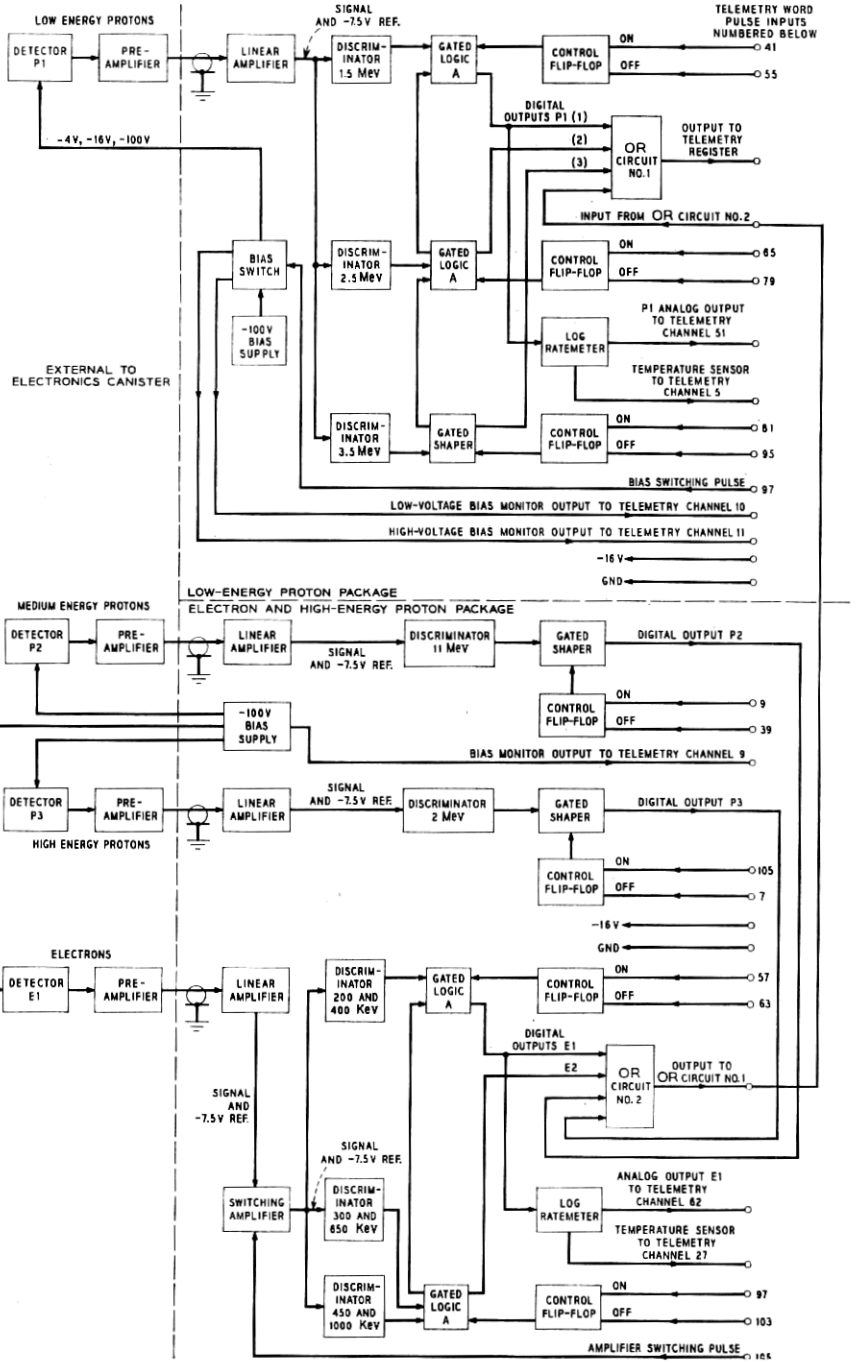

Fig. 17 — Radiation particle experiment block diagram.

+50°C with a period of 3 hours, while reverse bias of 120 v was cycling 20 minutes on and 1 hour off.

(d) Exposure to γ radiation at 50 rads/hr during bias cycling.

During all this testing and also during shelf-aging, accurate measurements of the reverse current-voltage characteristics were made frequently, as a very sensitive indication of surface stability. Only stable devices were selected for use.

4.3 *Electronic Circuits*

4.3.1 *Block Diagrams*

The electronic circuits of the radiation particle experiments are shown in block diagram form in Fig. 17. Each block represents the smallest part of a circuit that has an essentially independent function. The four detectors are at the left of the diagram. The function of the preamplifiers, which are to the right of the detectors, is to produce an output current pulse whose maximum is proportional to the charge produced in the detector by an incident particle. The linear amplifiers amplify this current pulse and present a proportionate output voltage pulse to one or more pulse amplitude discriminators. The discriminators produce an output current pulse of fixed shape for each input pulse above a threshold amplitude at the discriminator input. The gated logic and shaper circuits decide, for any input pulse, the highest discriminator threshold exceeded and produce an output pulse corresponding to that decision. The control flip-flops control the digital outputs and are turned "on" and "off" by signals from the telemetry timing circuits. Only one gated logic or shaper circuit is operative at any one time. All others are held off by their respective control flip-flop. The OR circuits combine all logic and shaper outputs on one output line to a register in the telemetry section. The log ratemeters take the average of the logarithm of the counting rate and present this average as a dc voltage to analog telemetry channels. A tristable multivibrator, bias switch and −100-volt bias supply provide three levels of bias to the low-energy proton detector.

Many of the problems encountered in the design of a satellite radiation measuring instrument are due to the random arrival of the particles and to their wide variation in energy. Problems of this nature are encountered in the analysis of the radiation from atomic nuclei and have been extensively treated in the literature.[22,23] In addition, electronic circuits for this application must be designed with adequate stability against changes in ambient temperature, supply voltage, and transistor parameters. Stability requirements are most severe in the linear amplify-

ing system and in the discriminators, where changes would shift the energy calibration of the experiment. In the amplifiers these requirements are met by the use of negative feedback through passive low-temperature coefficient elements in loops having large reserve gain.

Shifts in baseline with pulse rate are eliminated by using double RC differentiation to produce a bipolar pulse. The maximum counting rate of each experiment is limited to 100,000 pulses per second by the linear system shaping network and digital circuit recovery times.

Overload of the amplifying system by large input pulses is handled by arranging gains and bias so that overloads occur outside the feedback loops at the output of the preamplifier. The system quickly recovers from the overload with negligible baseline shift.

Electronic noise in the preamplifier is a limiting factor in the lowest energy of electrons that can be measured. A 25-Kev equivalent noise linewidth has been attained, a value well below the threshold of the lowest electron channel.

4.3.2 *Circuit Reliability*

With extended operation in space as a design goal, special attention was given to circuit reliability. Reliability has been enhanced through design simplicity, outstanding cases of which are the log ratemeters, bias supplies, and gated logic and shaper circuits which require only a single transistor to perform their function. Another method used to improve reliability was to design the system so that failure of a circuit would not terminate the entire experiment. The three proton experiments have been divided into independent parts so that the loss of one does not affect the operation of the others. In the low-energy proton and electron experiments, several independent discriminators enable collection of meaningful data even if a single discriminator fails. A -100-v bias supply common to three detectors is equipped with a diode OR circuit which, in the event of failure, would automatically switch in the -16-v satellite supply. Although performance would be limited at this reduced bias, useful data would still be received. Care was taken to avoid series failure mechanisms such as single power line filters and fuses. All circuits are separately decoupled and load limited.

4.3.3 *Linear System*

4.3.3.1 *Preamplifier.* The total detector output charge q_s produced by an incident particle is amplified in a linear system whose peak output voltage is proportional to q_s. A conventional method of doing this is

to amplify the voltage appearing across the total capacitance from input to ground. This voltage is

$$e_s = q_s/C_T$$

where e_s is the input signal voltage, and C_T is the total capacitance from the input to ground including the junction capacitance. In the solid-state detector, however, the junction capacitance changes with bias and ambient conditions, and consequently the voltage signal, e_s, would not always maintain the same relationship to the input charge.

An integrating preamplifier whose output is relatively unaffected by changes in detector capacitance is shown in Fig. 18.[24] The output voltage, e_o, is nearly equal to the input charge, q_s, divided by the feedback capacitance, C_F, if the open loop voltage gain is large. Thus the output signal is relatively insensitive to changes in detector capacitance. The preamplifiers in the Telstar satellite are of this type.

4.3.3.2 *Linear Amplifier.* After the preamplifier, the signal is amplified further in a linear current amplifier, which uses a two-transistor configuration described by Goulding.[25]

4.3.3.3 *Linear Signal Shaping.* The signal from the detectors is differentiated twice in the linear system with equal one-microsecond RC clipping networks, which are shown in Fig. 18. A resistor, R_C, of resistance such that R_CC_F equals one microsecond, is placed across the preamplifier feedback capacitor, C_F, to provide the first clip. A second clip is made by the combination of the output impedance of the preamplifier and a capacitor, C_C, between the preamplifier and the linear amplifier. The output resistance of the preamplifier is conveniently fixed

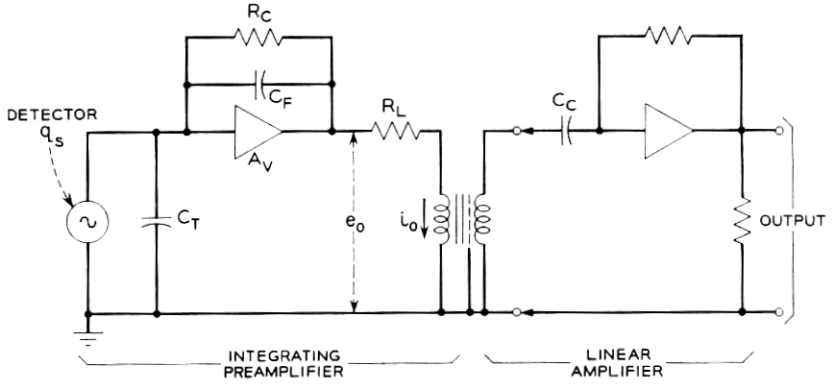

Fig. 18 — The linear system.

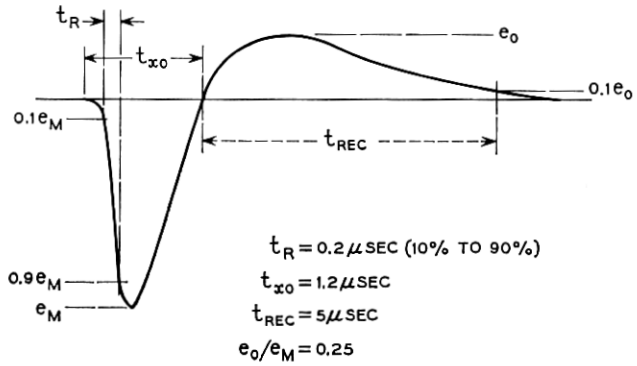

Fig. 19 — Linear amplifier output waveform.

by resistor R_L. The impedance looking into the input of the linear amplifier is very small (about 40 ohms), so it does not significantly affect the second clip time constant. The double-clipped signal as it appears at the linear amplifier output is shown in Fig. 19. The transformer at the output of the preamplifier contains an electrostatic shield to prevent coupling of common mode interference into the amplifier.

4.3.3.4 *Switching Amplifier.* The electron experiment, which is at the bottom of the block diagram, Fig. 17, has four levels of data but uses only two telemetry channels. This is accomplished by changing the gain of the linear amplifier system between successive telemetry frames. A plot of the electron channels for the electron analyzer is shown in Fig. 20. Three discriminators set the two channels shown by the solid lines.

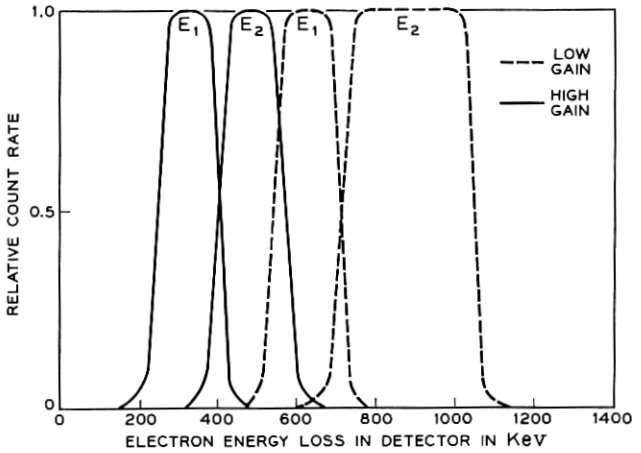

Fig. 20 — Response of electron channels as a function of input pulse height.

Decreasing the gain of the linear system shifts the energy thresholds up to those indicated by the dashed lines. In the satellite, the electron detectors count at one gain during a given telemetry frame and at another gain during the next frame.

The switching amplifier is shown in Fig. 21. The amplifier loop is similar to that of the ordinary linear amplifier. The gain of the amplifier is proportional to $1/R_4$ when transistor Q_3 is on, and $1/(R_4 + R_5)$ when Q_3 is off.

The switching transistor, Q_3, is driven by the bistable switch. The switching signal input is a timing signal from the telemetry package that occurs once each frame. An indication of the position of the bistable is telemetered.

4.3.4 *Digital System*

4.3.4.1 *Pulse Height Analyzers.* Two methods of pulse height analysis are conventionally used in random pulse height measurements: the stacked-discriminator method[22] and the pulse-height-to-time-converter method.[26] The relative simplicity of the stacked-discriminator analyzer was felt to be of commanding importance in this application.

In the stacked-discriminator analyzer each discriminator is biased at a different level or threshold. Any input pulse causes each discriminator whose threshold it exceeds to trigger and produce an output pulse. Since only the highest discriminator threshold exceeded is of interest,

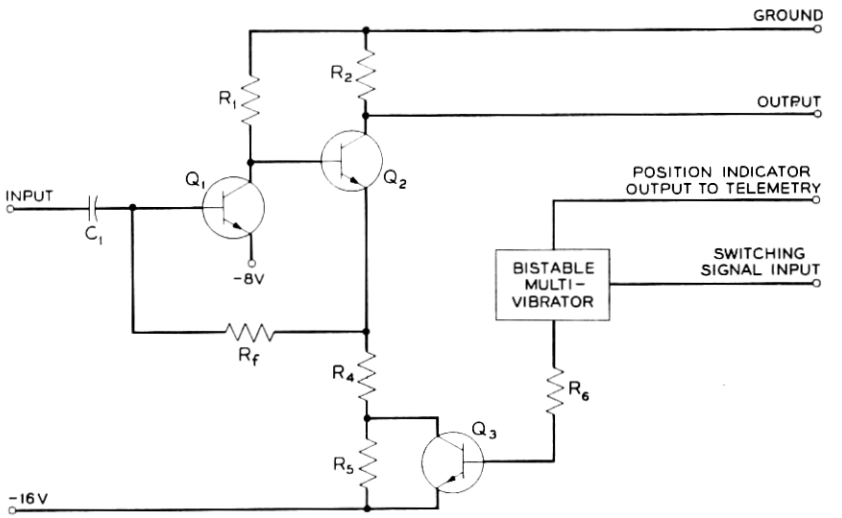

Fig. 21 — Switching amplifier (simplified).

logic circuits following the discriminators determine the one with the highest threshold that was triggered.

4.3.4.2 *Discriminator.* The characteristic most difficult to achieve in the design of a threshold discriminator for satellite use is thermal stability. The circuit used in the Telstar satellite (Fig. 22) is based on the emitter-coupled monostable multivibrator to take advantage of the inherent compensation of base-emitter voltage change with temperature. All other voltage drops that would affect threshold sensitivity are eliminated except an adjustable potential, V_t, that is derived from a zero temperature-coefficient reference element. An inductor, L_1, used instead of a base return resistor on the normally conducting transistor of the emitter-coupled pair, eliminates a temperature-sensitive voltage drop at that point.

A second-order effect on the threshold thermal stability is the variation of transistor beta with temperature. To trigger the multivibrator, the input signal must raise the base of Q_3, the normally "off" transistor, until its beta is large enough to produce a gain around the feedback loop of greater than one. At low temperatures the beta of Q_3 is reduced, so the input signal must be slightly larger than at higher temperatures. Nevertheless the discriminator threshold is quite stable. From $-50°C$ to $+50°C$ the threshold does not vary more than ± 1 per cent. The discriminator output, taken from the collector of Q_3, is a current pulse of about 600 μa, with a duration determined mainly by the shape of the input pulse.

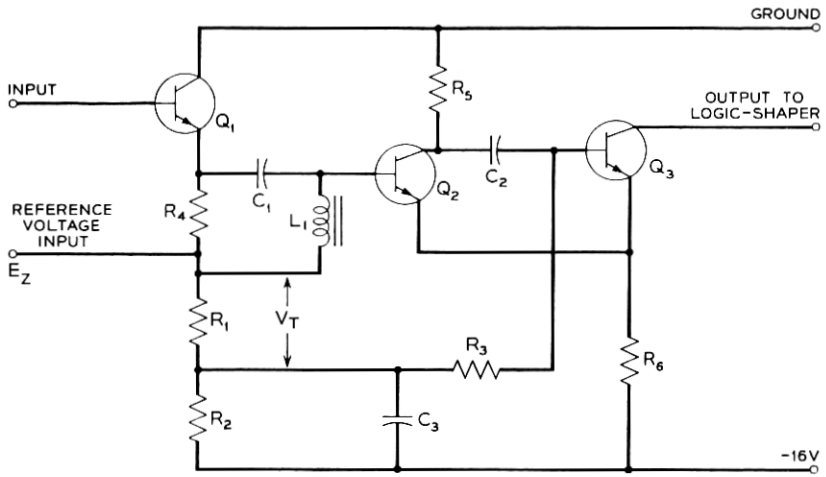

Fig. 22 — Discriminator circuit.

4.3.4.3 *Gated Logic Circuit.* The gated logic circuits have two functions: first, to determine the discriminator with the highest threshold that was triggered by a signal from the linear system; second, to produce an output pulse suitable for driving a coaxial cable and a register. Each discriminator's output is trying to turn a gated logic circuit on while at the same time keeping the one below it from turning on. A discriminator turns on a logic circuit only if the next higher discriminator does not produce an output during the rise of the pulse from the linear amplifier driving them. Since the input pulse has a finite rise time, a discriminator with a higher threshold will trigger later than one with a lower threshold. The logic circuit must delay its decision until the higher discriminators have had time to fire.

These operations are performed in an unusual manner in a modified blocking oscillator, shown in Fig. 23. Two input windings of a pulse transformer connect to the discriminator outputs, and a third winding that has the same number of turns as the input windings connects to the transistor base. The current in the base winding is the algebraic sum of the current in the input windings as long as the transistor is turned off. Winding 1 is connected to the upper discriminator in the direction that produces a base winding current that drives the base of Q_1 negative. Winding 2 is connected to the lower discriminator in the opposite phase; when this discriminator fires, the base of Q_1 goes positive.

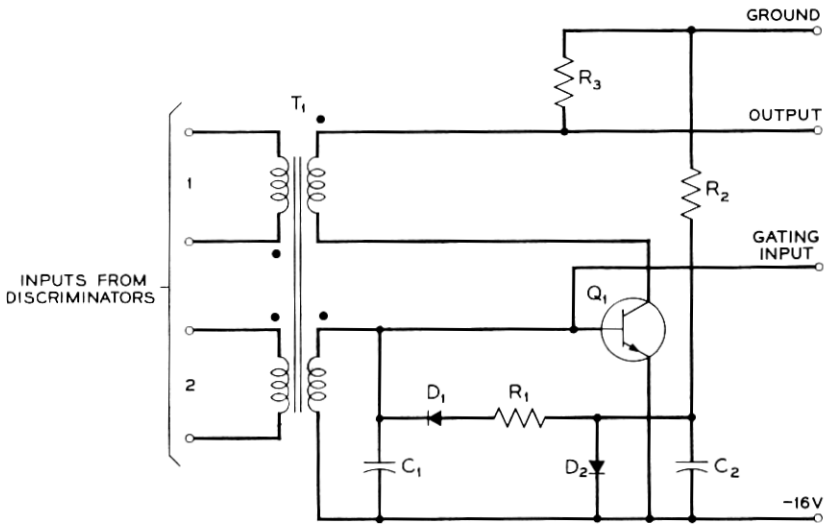

Fig. 23 — Logic-shaper circuit.

When the input pulse is large enough to trigger the lower but not the upper of two discriminators connected to a gated logic unit, the current pulse pours into C_1 and charges it linearly with time. Transistor Q_1 is normally biased off by holding the base at the emitter voltage. The capacitor C_1 must then charge to about 0.7 v before the transistor turns on. In the circuit shown, the input current from a discriminator is about 600 μa. The time required to charge the capacitor to 0.7 v is about 0.5 μsec, allowing the input pulse to rise to the next discriminator threshold if it will. If the next higher discriminator were to trigger during this 0.5-μsec period, its output current, pouring in the other input winding, would prevent the capacitor from charging enough to turn on Q_1.

When Q_1 does turn on, it operates as a blocking oscillator. Current in the collector circuit is fed back to the base and the transistor rapidly saturates. The saturation current is limited to about 2 ma by R_3. The inductance of the collector winding is such that the transistor is held on in saturation for about 4 μsec. Then Q_1 turns off and the energy stored in the transformer inductance is dissipated in resistor R_1, which is chosen to slightly underdamp the overshoot. With this damping the blocking oscillator is completely recovered in about 10 μsec. Diode D_1 prevents R_1 from taking any of the 600 μa charging current; diode D_2 biases diode D_1 so that R_1 is effective for the entire negative swing in the base circuit. Fig. 24(a) shows the base waveform for both conditions of operation: when just one discriminator fires (solid line), the capacitor charges linearly until the blocking oscillator fires; when both

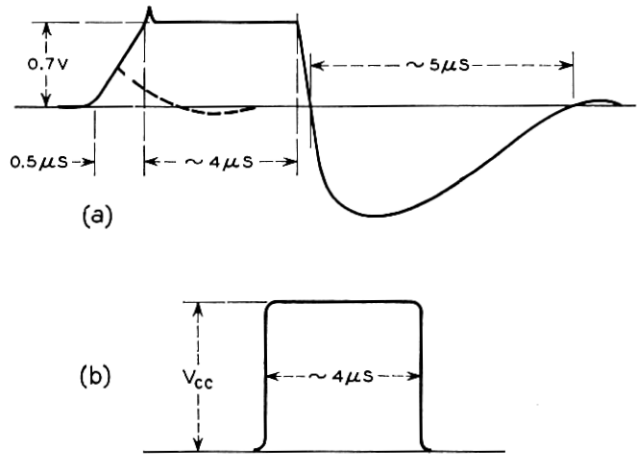

Fig. 24 — Logic shaper waveforms: (a) base waveform (b) output waveform.

discriminators fire (dashed line), the charge of the capacitor is stopped before the blocking oscillator fires. The shaper circuits are similar to the logic circuits, the chief difference being that only one input is provided. Fig. 24(b) shows the output waveform.

A 14-bit register[2] is provided in the telemetry package to accumulate the pulses from the radiation circuits. Time sharing of the outputs of the logic and shaper circuits into this register is accomplished by holding off all except one with saturating transistor gates connected between the gating inputs and −16 v. The gates are controlled by flip-flops shown in the block diagram. The flip-flops are switched by signals from the telemetry timing circuit. The timing is indicated by the telemetry word number given on the block diagram. Two word times are allowed between each counting period for read-out of the telemetry register. The OR circuits which combine all outputs onto one line are simply diode OR's and an emitter follower.

4.3.4.4 *System Response to Closely Spaced Pulses.* The handling of closely spaced pulses by the analyzer and linear system is somewhat complicated. Pulses further apart than about 7 μsec are essentially independent, since the system will have had time to recover sufficiently between them. (The 7 μsec limitation occurs in the logic circuit.) A pulse that occurs between 7 μsec and about 2 μsec after another is reduced in amplitude by the "undershoot" of the first pulse in the linear system as shown in Fig. 19. (The 2-μsec time is the recovery time of the discriminator.) If the reduced second pulse falls in a different channel than the first pulse it will be counted, but if it falls in the same channel as the first pulse it will not count, since the logic unit has not recovered from counting the first pulse. Signals that occur from 2 μsec to 0.6 μsec after a first pulse are distorted by the first pulse and are counted if their amplitude is sufficiently higher than the first pulse to trigger a discriminator that was not triggered by the first pulse. These signals (2.0 μsec to 0.6 μsec) cannot trigger discriminators that were triggered by the first pulse, since they have not sufficiently recovered. Signals occurring closer together than 0.6 μsec are indistinguishable and are counted as a single pulse that is larger than either of them. These effects are not considered as serious limitations on the system's performance in its intended application.

4.3.5 *Log Ratemeter*

The radiation experiment telemetry register has a capacity of 14 bits (16,383 counts). Whenever the register has filled and input pulses are still entering, it returns to zero and continues to count. In a region of

high activity the register may "overflow" several times, leaving an uncertainty in the total count. A log ratemeter[27] is used on the most sensitive levels to determine how many times the register has filled; during normal periods it provides redundancy. This circuit, which produces an output voltage that increases approximately as the log of the input pulse rate from 1 to 100,000 pps, contains a blocking oscillator which is triggered by the output of the logic circuit. The oscillator completely discharges a bank of five capacitors, differing by factors of 20, each time it fires. Isolating diodes enable the capacitors to discharge simultaneously but charge individually through large identical series resistors. Charging currents for the capacitors are added and integrated to produce an analog output voltage. This voltage is coupled to an analog telemetry channel, which is read out just before the digital information from the level to which the ratemeter is connected. The output is the average of the logarithm of the counting rate, an important consideration in the case of rapidly varying random pulse rates. A typical plot of output voltage vs input rate is shown in Fig. 25.

4.3.6 *Detector Bias*

4.3.6.1 *100-volt Bias Supply.* The −100-v bias supply is basically a free-running blocking oscillator driving a transformer with a 10:1 tertiary winding. The resulting high voltage is rectified and RC-filtered

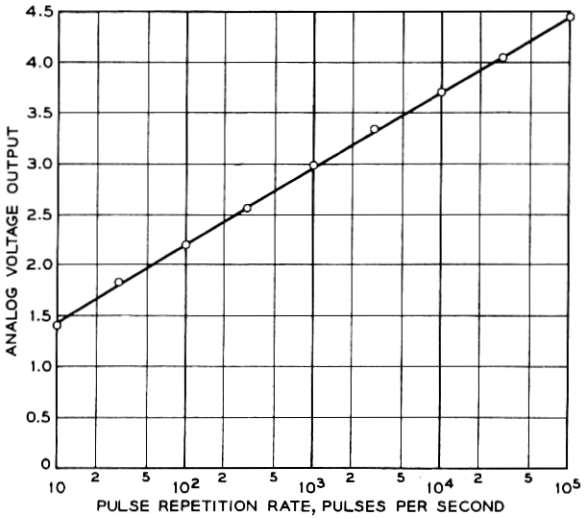

Fig. 25 — Ratemeter response.

in a conventional manner. However, the method by which load regulation is obtained is rather unique. DC feedback from a high-resistance divider on the output controls the oscillator repetition rate in proportion to the load by determining the charging time of a capacitor in the oscillator base circuit.

The detector load is nominally less than one microampere; load regulation is 0.1 per cent per microampere for loads up to 100 microamperes. Temperature stability is 0.05 per cent per degree centigrade.

4.3.6.2 *Tristable Multivibrator and Bias Switch.* The low-energy proton detector operates sequentially at three levels of bias. The tristable multivibrator circuit controls the position of the bias switch. A timing signal from the telemetry package switches the state of the tristable once each frame. The bias switch consists of transistor gates which turn off the −100-v bias supply and set the other levels of bias.

All three bias levels are monitored by an analog telemetry channel.

4.3.7 *Construction*

The detectors and their preamplifiers are mounted on the outer framework, with three of the four detectors protruding into space through holes in the satellite skin. The remainder of the radiation circuitry is located within the temperature-controlled electronics canister.

With the exception of the preamplifiers, the radiation electronics in the Telstar satellite are constructed in modules,[28] each represented by a square in the block diagram, Fig. 17. These modules consist of fiber glass epoxy circuit board wafers forming the top and bottom of a sandwich with components stacked like cordwood between them. Leads extend through a "mother board" on which all modules are mounted and interconnected. The entire subassembly is encapsulated in polyurethane foam, giving it good rigidity with little added weight. The radiation circuit is divided into two subassemblies to facilitate placement among the communications equipment complex within the canister.

V. PERFORMANCE IN SPACE

All parts of the radiation experiment have performed in space as expected and have provided a wealth of data, part of which will be described in a separate paper in this issue. The particle detectors, which are potentially susceptible to changes in their characteristics due to radiation surface effects,[21] have shown an internal consistency which indicates their continuing satisfactory operation after several months in space. This is true in spite of the higher radiation intensity encountered than

had been anticipated, and in spite of the often extensive periods of continuous bias under which the devices have been in operation, a condition which aggravates the radiation surface effects.

VI. ACKNOWLEDGMENTS

A large number of people have participated in an important way in this work. We wish in particular to acknowledge the contributions of: G. H. Wheatley, J. W. Rodgers, J. J. Darold and P. V. Chase in the development, production and testing of the particle detectors; W. M. Augustyniak in calibration of the detectors; B. H. McGahey in the development of the aspect and radiation damage solar cells; and D. J. D'Stefan, T. E. Davis, M. F. Slana, R. R. Blair and D. G. DeNure in the development and testing of the radiation damage transistors.

REFERENCES

1. Smith, K. D., Gummel, H. K., Bode, J. D., Cuttriss, D. B., Nielsen, R. J., and Rosenzweig, W., The Solar Cells and Their Mounting, B.S.T.J., this issue, Part 3.
2. Chapman, R. C., Jr., Critchlow, G. F., and Mann, H., The Telemetry and Command Systems, B.S.T.J., this issue, p. 1027.
3. Hutchison, P. T., and Swift, R. A., Results of *Telstar* Satellite Space Experiments, B.S.T.J., this issue, Part 2.
4. Brown, W. L., Gabbe, J. D., and Rosenzweig, W., Results of the *Telstar* Radiation Experiment, B.S.T.J., this issue, Part 2.
5. Gummel, H. K., and Smits, F. M., Testing of Solar Cells by Means of Spectral Analysis, Proc. of the Solar Working Group Conference, **2,** February 27, 28, 1962, pp. 3–17.
6. Loferski, J. J., and Rappaport, P., Radiation Damage in Ge and Si Detected by Carrier Lifetime Changes: Damage Thresholds, Phys. Rev., **111,** March, 1958, p. 432.
7. Easley, J. W., and Dooley, J. A., Fast Neutron Bombardment Reduction of Transistor Current Gain, J. Appl. Phys., **31,** June, 1960, p. 1024.
8. Freden, S. C., and White, R. S., Protons in the Earth's Magnetic Field, Phys. Rev. Letters, **3,** July 1, 1959, p. 9.
9. Van Allen, J. A., *Space Research*, Ed. H. K. Kallman Bijl, North Holland Publishing Co., Amsterdam, 1960, pp. 749–750.
10. Singer, S. F., Nuclear Explosions in Space, Nature, October 27, 1962, p. 301.
11. Brown, W. L., Introduction to Semiconductor Particle Detectors, I.R.E. Trans. Nuc. Sci., **NS-8,** 1961, pp. 2–10.
12. Blankenship, J. L., and Borkowski, C. J., Performance of Silicon Surface Barrier Detectors with Charge Sensitive Preamplifiers, I.R.E. Trans. Nuc. Sci., **NS-7,** 1960, p. 185.
13. Miller, G. L., Brown, W. L., Donovan, P. F., and MacIntosh, I. M., Silicon p-n Junction Particle Detectors, I.R.E. Trans. Nuc. Sci., **NS-7,** 1960, p. 185.
14. See I.R.E. Trans. Nuc. Sci., **NS-8,** January 1, 1961, and **NS-9,** June 1, 1962.
15. Pell, E. M., Ion Drift in an n-p Junction, J. Appl. Phys., **31,** February, 1960, pp. 291–302.
16. Monteith, L. K., M.S. thesis, Duke University, 1962.
17. McKenzie, J. M., and Ewan, G. T., Semiconductor Electron Detectors, I.R.E. Trans. Nuc. Sci. **NS-8,** 1961, pp. 50–53.
18. Buck, T. M., Proceedings of the Asheville Conference on Semiconductor Nuclear Particle Detectors, Dabbs, J. W. T., and Walter, F. J., Editors, NAS-NRC Pub. 871, 1961, p. 111.

19. Buck, T. M., and McKim, F. S., Effects of Certain Chemical Treatments and Ambient Atmospheres on Surface Properties of Silicon, J. Electrochem. Soc., **105,** December, 1958, pp. 709–714.
20. Buck, T. M., Wheatley, G. H., and Rodgers, J. W., to be published.
21. Peck, D. S., Blair, R. R., Brown, W. L., and Smits, F. M., Surface Effects of Radiation on Transistors, B.S.T.J., **42,** January, 1963, p. 95.
22. Elmore, W. C., and Sands, M., *Electronics*, McGraw-Hill, New York, 1949, pp. 241–249.
23. Chase, R. L., *Nuclear Pulse Spectrometry*, McGraw-Hill, New York, 1961, 22 pages.
24. Kelly, G. A., I.R.E. National Convention Record, Part 9, 1957, p. 63.
25. Goulding, F. S., Transistorized Radiation Monitors, I.R.E. Trans. Nuc. Sci., **NS-5,** 1958, pp. 38–43.
26. Wilkinson, D. H., Stable Ninety-Nine Channel Pulse Amplitude Analyzer for Slow Counting, Proc. Cambridge Phil. Soc., **46,** Part 3, 1950, p. 508.
27. Cooke-Yarborough, E. H., Counting-Rate Meter of High Accuracy, Proc. Inst. Elec. Engrs., London, 1951, p. 196.
28. Shennum, R. H., and Haury, P. T., A General Description of the *Telstar* Spacecraft, B.S.T.J., this issue, p. 801.